Mécanique & Industries 11, 477–488 (2010)
www.mecanique-industries.org
Mécanique & Industries

DOI: 10.1051/meca/2010043

Experimental investigation of air bearings dynamic coefficients

Pierre Matta[a], Laurent Rudloff and Mihai Arghir

Institut PPRIMME, UPR 3346, Université de Poitiers (anciennement Laboratoire de Mécanique des Solides), Boulevard Marie et Pierre Curie, Téléport 2, BP 30179, 86962 Futuroscope Chasseneuil Cedex, France

Received 25 February 2010, Accepted 7 June 2010

Abstract – The paper presents the experimental work developed by the authors for the identification of rotordynamic coefficients of air bearings. Air bearings work at very high rotation speeds and are known to have nonlinear dynamic characteristics depending at least on the excitation frequency. The paper presents two very similar test rigs, the testing procedure and the algorithm for identifying the rotordynamic coefficients. The test rigs consist of a rigid rotor guided by fixed bearings and driven by a spindle. The dynamic loads are applied by two orthogonally mounted shakers applying two linear independent excitations. Two air bearings are analysed in the present paper. The test procedure is first developed for a simple circular bearing with easily predictable dynamic characteristics. Its rotordynamic coefficients are identified by using a least square procedure based on rational functions. The coefficients are compared to theoretical results in order to underline the limits of the identification algorithm. The procedure is next applied to a first generation foil bearing. Rotordynamic coefficients are presented for different working conditions (static loads and rotation speeds) and are discussed comparing them to circular air bearings.

Key words: Air bearings / dynamic modelling / identification

Résumé – Étude expérimentale des coefficients dynamiques des paliers à air. Cette étude présente une démarche expérimentale pour identifier les coefficients dynamiques des paliers à air. Les paliers à air fonctionnent à des grandes vitesses de rotation et sont réputés pour leur comportement dynamique considérablement non linéaire dépendant au moins de la fréquence de rotation. Cet article présente deux dispositifs d'essai similaires, la procédure expérimentale et l'algorithme d'identification des coefficients dynamiques. Les bancs d'essai sont constitués d'un arbre rigide supporté par des paliers fixes et entraîné par une broche. Les forces dynamiques sont appliquées par deux pots vibrants appliquant deux excitations linéairement indépendantes suivant deux directions orthogonales. Dans cette étude deux types de palier à air ont été étudiés. La procédure expérimentale a été développée pour un palier cylindrique simple dont les coefficients dynamiques sont aisément calculés. Les coefficients dynamiques du palier cylindrique ont été identifiés à l'aide d'une méthode des moindres carrés basée sur des fonctions rationnelles. Ces résultats sont comparés avec la théorie pour souligner les limites de la procédure d'identification. La méthode d'identification est ensuite appliquée pour des paliers à feuilles, de la première génération. Les coefficients dynamiques sont présentés pour plusieurs conditions de fonctionnement (charge statique et vitesse de rotation) et sont comparés avec les résultats obtenus pour des paliers cylindriques.

Mots clés : Palier à air / modélisation dynamique / identification

1 Introduction

Non-pressurized air bearings are designed to work with no additional lubricant. In the case of circular bearings or foil bearings, the air lift force is created by the rotation of the journal relative to the journal. These air bearings called aerodynamic bearings are characterized by a small film thickness and can be used in turbomachinery when high rotational speeds are required. Meanwhile, air bearings have very low damping characteristics. Foil bearing represents a special technology based on a compliant structure intended to increase damping to the traditional low-damped air bearing by adding Coulomb friction. Due to the air compressibility, aerodynamic bearings are non-linear components being characterized by frequency dependent dynamic coefficients. In addition,

[a] Corresponding author:
pierre.matta@lms.univ-poitiers.fr

Nomenclature

A_0, A_1, B_0	parameters of the transfer function
a_{ij}	acceleration [m.s^{-2}]
$A_{ij}(\omega)$	FFT of $a_{ij}(t)$
C_{ij}	damping [Ns.m^{-1}]
D	bearing diameter [m]
f_i	force [N]
$F_i(\omega)$	FFT of $f_i(t)$
H	transfer function
K_{ij}	stiffness [N.m^{-1}]
L	bearing length [m]
M	housing mass [kg]
n	number of tests
W	load [N]
x, y	displacement defined in Figure 3 [m]
X, Y	displacement in excitation directions [m]
$Z = K + j\omega C$	impedance [N.m^{-1}], $j = \sqrt{-1}$
Ω	rotation angular velocity [rad.s^{-1}]
ω	perturbation angular velocity [rad.s^{-1}]
Superscripts	
$\dot{x}$, $\ddot{x}$	time derivative
Subscripts	
$i, j = X, Y$	or $i, j = x, y$

due to the compliant structure, foil bearings present even more nonlinear dynamic characteristics than circular air bearings involving large displacements and Coulomb friction between foils while dynamically loaded.

Many theoretical studies were developed to predict the dynamic behavior of aerodynamic bearings [1–6]. Recently, experimental investigations were developed to verify theoretical results. Ertas et al. [7,8], Rudloff et al. [9] and Matta et al. [10] detailed the design of high speed test rigs dedicated to gas lubricated journal bearings. These "floating bearing" test rigs are able to measure the frequency dependent rotordynamic coefficients.

The present work investigates the dynamic characteristics of a simple circular bearing of 40 mm diameter and of a first generation foil bearing of 38 mm diameter. Both bearings have $L/D = 1$.

2 Experimental set-up

Experimental investigations are first developed for a simple circular bearing with easily predictable dynamic characteristics before extending the experimental procedure to characterize air foil bearings. Therefore, two very similar test rigs were developed using the same floating bearing design.

2.1 Circular bearing test rig

Figure 1 depicts a layout of the first air bearing test facility presented in detail by Matta [10]. The test rig consists of a high speed shaft supported on two identical water lubricated hybrid bearings of Lomakin type and driven by a spindle (60 krpm, 8 kW), while the tested bearing is mounted floating at the non-drive end of the shaft.

The floating bearing design is based on the assumption that its housing is free to move in the excitation directions while the shaft is considered as fixed. Therefore, the water lubricated hybrid bearings presented in Figure 2 are designed to have a very high stiffness. This stiffness is obtained by feeding the bearings with pressurized water up to 7.5 MPa. The radial clearance is about 50 μm and the length of each of the two Lomakin bearings is $L = 30$ mm (Fig. 2). Due to its high feeding pressure, the Lomakin hybrid bearing is characterised by high radial stiffness estimated at 2.8×10^7 N.m^{-1} for 5.5 MPa of water feeding pressure. In addition, the use of two largely spaced Lomakin bearings confers to the resulting hybrid bearing a relatively large tilting stiffness. Pressurized water is injected into the circumferential feeding groove via 4 orifices angled at 85° against shaft rotation. The angled injection assures a very low cross coupling stiffness and therefore, no self sustained instability was detected in this bearing up to 55 krpm. The rotor is 350 mm long, and, following numerical estimations, the first natural frequency of its free-free beam mode is 1250 Hz. The rotor can then be considered rigid for speeds enabled by the spindle (<60 krpm).

The identification method consists in measuring the response of the floating bearing to external excitations for each working condition (static load and rotational speed). Static loads are applied vertically by a spring and measured by a dynamometer while dynamic excitations are applied in two orthogonal directions by two identical electromagnetic shakers. The tested bearing is mounted in a housing (Fig. 3) equipped with four inductance proximity probes (two in each end plane) measuring the relative displacements between the shaft and the bearing in the excitation directions and four accelerometers (two in each bearing end plane assisting the proximity probes). The stinger of each shaker is provided with a dynamic force sensor. The rotation speed is measured by an optic keyphasor. To avoid the dynamic misalignment problem exhibited at previous testing [10], the bearing housing is mounted on three flexible stingers fitted in the base plate. The measured stiffness of the squirrel cage is 15.6 kN.m^{-1}, largely lower than the expected stiffness of the tested bearings. The goal of this experimental facility is to identify dynamic coefficients of a circular air bearing of 40 mm diameter. The circular bearing is made of graphite contained in a stainless steel sleeve. The bearing and its geometric characteristics are given in Figure 4.

2.2 Foil bearing test rig

The first set of analyses performed with the simple circular bearing, enabled the development of an experimental procedure and confirmed the identification method. The second objective of the experimental investigation is the identification of dynamic coefficients

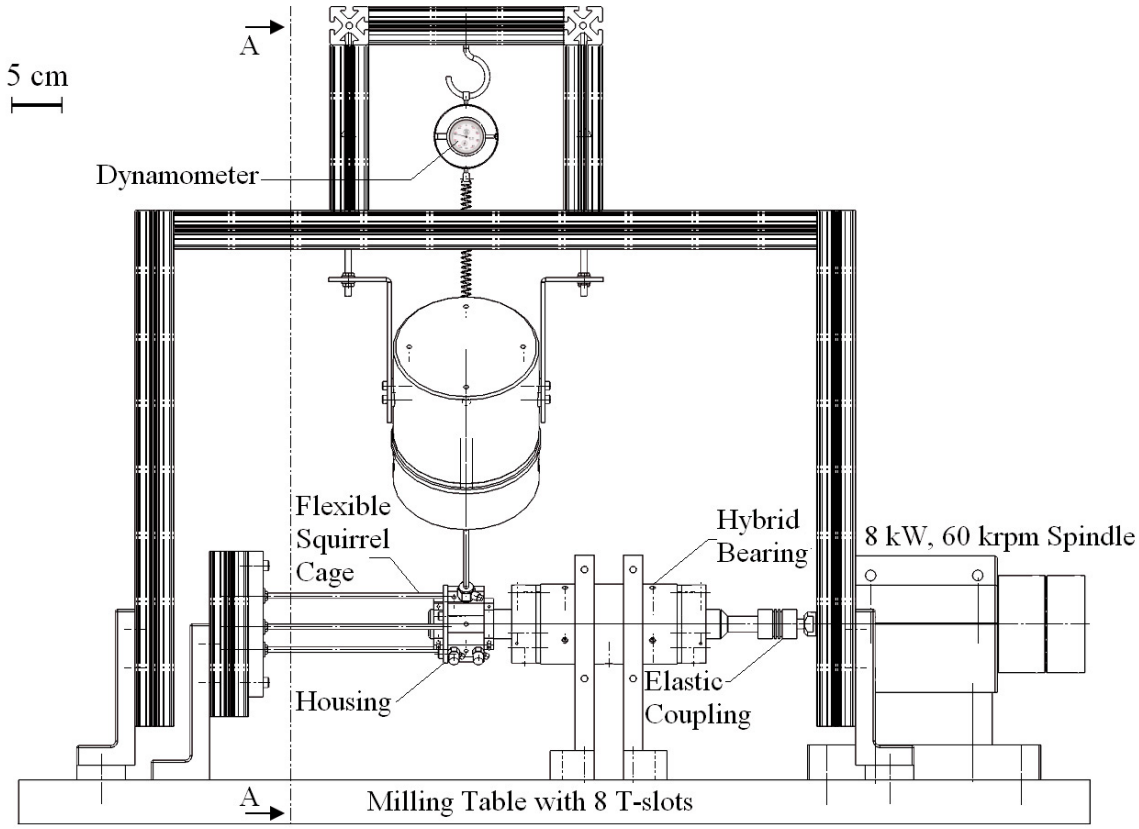

Fig. 1. Primary test rig layout.

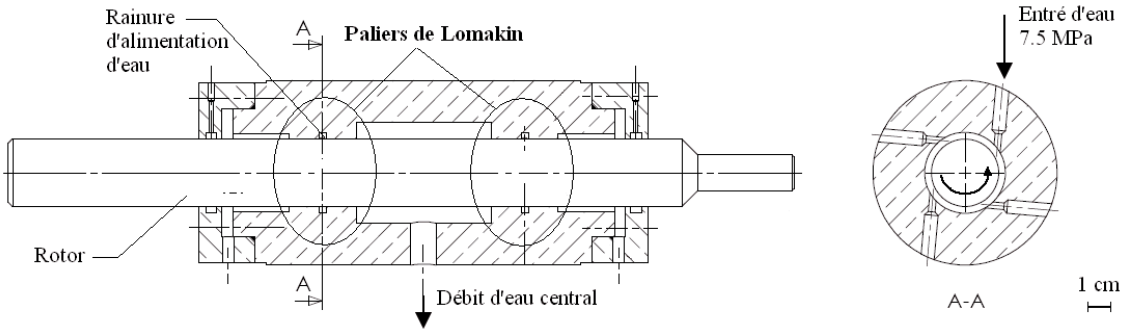

Fig. 2. Layout of the double Lomakin hybrid bearing with eight counter-rotating injections.

of a generation 1 commercial foil bearing of 38 mm diameter. The bearing and its geometric characteristics are given in Figure 6. A second test rig (Fig. 5) dedicated exclusively for foil bearing analysis was initiated by Le Lez [1] and was continued by Rudloff et al. [9]. The main difference between this test rig and the one depicted in Figure 1 is the position of the tested bearing housing. The floating bearing is mounted on the rigid rotor at a position midway between the supports components which consist of two lifelong grease lubricating high speed ceramic ball bearings. The maximum allowable speed of the 1 kW spindle drive is about 40 krpm. The static load, the dynamic excitations as well as the instrumentation of the bearing are similar to the first test rig.

3 Input/output signal processing

Periodic forces with different excitation frequencies are applied in X and Y direction (Fig. 3). In order to avoid non linear effects and to have significant displacement at each excitation frequency, the dynamic loads were separately applied for each frequency in the spectrum without combining the excitations in a single signal. The dynamic excitation applied on the housing by the electromagnetic shaker is a periodic force commanded by an external amplifier with a simple sinusoidal input signal characterized by a given frequency. The amplitude of the dynamic load is then measured by the force sensors.

It must be taken into account that all measured signals contain an inherent synchronous excitation due to

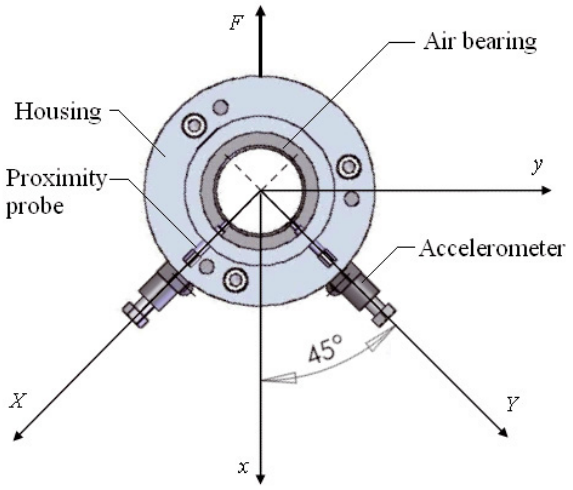

Fig. 3. System of coordinates represented on the bearing housing.

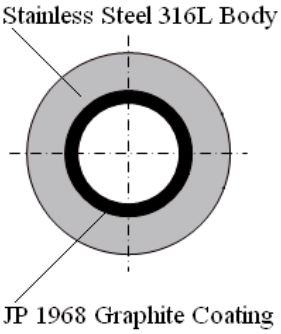

Bearing length [mm]	*40*
Bearing diameter [mm]	*40*
Clearance [μm]	*32*
Graphite thickness [mm]	*3*

Fig. 4. Tested circular bearing.

shaft runout (manufacturing tolerances) and/or residual unbalance. The identification of bearing dynamic coefficients requires response signals free from runout. The runout filtering is therefore performed by subtracting all components of the phase corrected FFT of the runout signal from the phase corrected FFT of each signal recorded with periodic excitation. The keyphasor of test rig enables the measurement of the rotation speed and represents a reference for measuring the phase angles of all signals.

During data acquisition, the sampling frequency must be high enough to satisfy the conditions of the Nyquist-Shannon sampling theorem but moderate to avoid excessive storage. Therefore, for the present experimental investigation, all signals were simultaneously sampled at 8192 samples.s^{-1} over 1 s. This yields a sample size of 8192 samples per channel and a frequency resolution of 1 Hz.

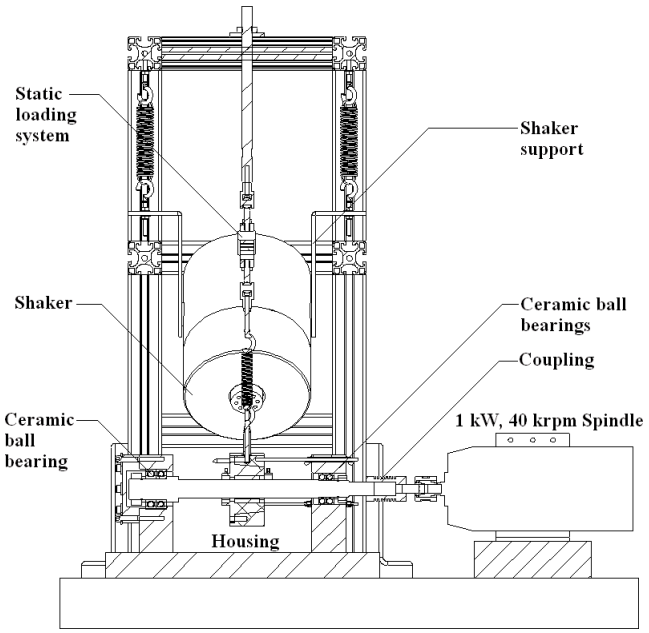

Fig. 5. Foil bearing test rig layout.

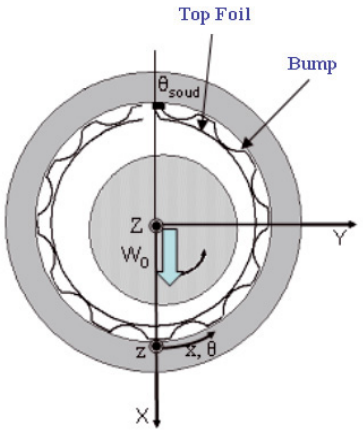

Bearing length [mm]	*38.1*
Bearing diameter [mm]	*38.1*
Clearance [μm]	*31.8*
Numbers of bumps	*26*
Top foil welding angle	*180°*
Foil thickness [μm]	*102*
Pitch [mm]	*4.572*
Bump half length [mm]	*1.778*
Initial bump height [mm]	*0.508*

Fig. 6. Tested foil bearing.

4 Rotordynamic coefficients identification method

The two test rigs present no significant differences, thus the same identification procedure will be used. The procedure used for identifying the dynamic coefficients is based on the use of the frequency domain experimental technique. If the dynamic force is applied only in

X direction, the dynamic equation of the quasi-floating bearing is:

$$M\begin{Bmatrix}\ddot{X}\\ \ddot{Y}\end{Bmatrix} = -\begin{bmatrix}C_{XX} & C_{XY}\\ C_{YX} & C_{YY}\end{bmatrix}\begin{Bmatrix}\dot{X}\\ \dot{Y}\end{Bmatrix} - \begin{bmatrix}K_{XX} & K_{XY}\\ K_{YX} & K_{YY}\end{bmatrix} \times \begin{Bmatrix}X\\ Y\end{Bmatrix} + \begin{Bmatrix}f_X\\ 0\end{Bmatrix} \quad (1)$$

where X and Y are the excitation directions (Fig. 3). The transformation of Equation (1) to the frequency domain introduces the dynamic coefficients of the bearing as components of the impedance functions $Z_{ab} = K_{ab} + j\omega C_{ab}$ and yields:

$$M\begin{Bmatrix}A_X(\omega)\\ A_Y(\omega)\end{Bmatrix} + \begin{bmatrix}Z_{XX}(\omega) & Z_{XY}(\omega)\\ Z_{YX}(\omega) & Z_{YY}(\omega)\end{bmatrix}\begin{Bmatrix}X(\omega)\\ Y(\omega)\end{Bmatrix} = \begin{Bmatrix}F_X(\omega)\\ 0\end{Bmatrix} \quad (2)$$

For each working condition, two independent excitations are sequentially applied in X and Y direction leading to the following linear system:

$$\begin{bmatrix}XX(\omega) & YX(\omega) & 0 & 0\\ 0 & 0 & XX(\omega) & YX(\omega)\\ XY(\omega) & YY(\omega) & 0 & 0\\ 0 & 0 & XY(\omega) & YY(\omega)\end{bmatrix}\begin{Bmatrix}Z_{XX}(\omega)\\ Z_{XY}(\omega)\\ Z_{YX}(\omega)\\ Z_{YY}(\omega)\end{Bmatrix} = \begin{Bmatrix}F_X(\omega) - MA_{XX}(\omega)\\ -MA_{YX}(\omega)\\ -MA_{XY}(\omega)\\ F_Y(\omega) - MA_{YY}(\omega)\end{Bmatrix} \quad (3)$$

In order to reduce the signal noise, the tested bearing is excited ten times in each direction. The impedances are then calculated by averaging the results streaming from the linear system (3):

$$Z(\omega) = \frac{1}{10}\sum_{n=1}^{10} Z_n(\omega) \quad (4)$$

At this step, rotordynamic coefficients are defined in the coordinated system of the shakers (X, Y). A 45° rotation enables to express them in a coordinate system linked to the static load (x, y).

Dynamic coefficients can be identified directly from the complex impedances, $K_{ij} = \mathrm{Re}(Z_{ij})$, $C_{ij} = \mathrm{Im}(Z_{ij})/\omega$. Nevertheless a better identification procedure is obtained by injecting all the measured impedances in a least square approach. If the dynamic coefficients don't depend on the excitation frequency, the least square approach is based on a second order polynomial curve fit [11] or an instrumental variable method [12]. However, when a large frequency-dependence is expected, a different curve fitting procedure is needed to obtain a smooth curve of the frequency dependent stiffness and damping coefficients. The idea is to consider the compressible air film as a viscoelastic material [13–18]. The first order transfer function for a viscoelastic model of the squeezed gas film yields:

$$H_x(s) = \frac{\Delta x(s)}{\Delta F(s)} = \frac{B_0 + s}{A_0 + sA_1} \quad (5)$$

where s is the Laplace transform and A_0, A_1 and B_0 are constant coefficients. The equivalence between the Fourier and the Laplace transforms for a sinusoidal perturbation $(s = j\omega)$, permits to write the complex impedance obtained by Equation (4) as a first order transfer functions Equation (5):

$$Z(\omega) = K + j\omega C = \frac{A_0 + j\omega A_1}{B_0 + j\omega} \quad (6)$$

One should mention that the transfer function represented in Equation (6) is only an approximation of complex impedances by rational functions. The calculation of A_0, A_1 and B_0 by a nonlinear minimization method leads to a smooth fitting curve of the frequency dependent stiffness and damping coefficients.

$$K(\omega) = \frac{A_0B_0 + \omega^2 A_1}{B_0^2 + \omega^2}, \quad C(\omega) = \frac{A_1B_0 - A_0}{B_0^2 + \omega^2} \quad (7)$$

5 Results

5.1 Bearing stability

A start-up check is necessary before any dynamic test. This check consists to measure the imbalance response of a slightly loaded bearing during its acceleration phase. The objective is to establish the static load that ensures a stable behavior of the bearing in the range of tested speeds. This concern is motivated by the fact that in some cases, air bearings can generate self induced vibrations. These vibrations are independent of dynamic excitations applied on the housing. They appear at a frequency just about half of the rotational speed (0.5 Ω) and are produced by an internal mechanism of the fluid which transforms the rotational energy to vibration energy.

Figure 7 presents the displacement response of the circular bearing (X direction) to rotor angular velocities between 70 and 500 Hz for 15 N static load. The waterfall plot depicts the appearance of a 100 Hz subsynchronous vibration when the rotation speed is 200 Hz. By increasing the rotation speed, the frequency of self induced vibrations increases progressively but remains approximately equal to 0.5 Ω (fluid whirl). When the rotational speed reaches 280 Hz, self induced vibrations frequency is approximately equal to 140 Hz and this frequency remains constant even after the rotor accelerates over 280 Hz. In this case, the generated vibrations called "fluid whip" takes over the fluid whirl. This phenomenon appears when the shaft reaches a speed equal to the double of the natural frequency of a test rig component. By referencing to [19], 140 Hz corresponds to the first natural frequency of rotor – hybrid bearing system which explains the source of the whip vibrations.

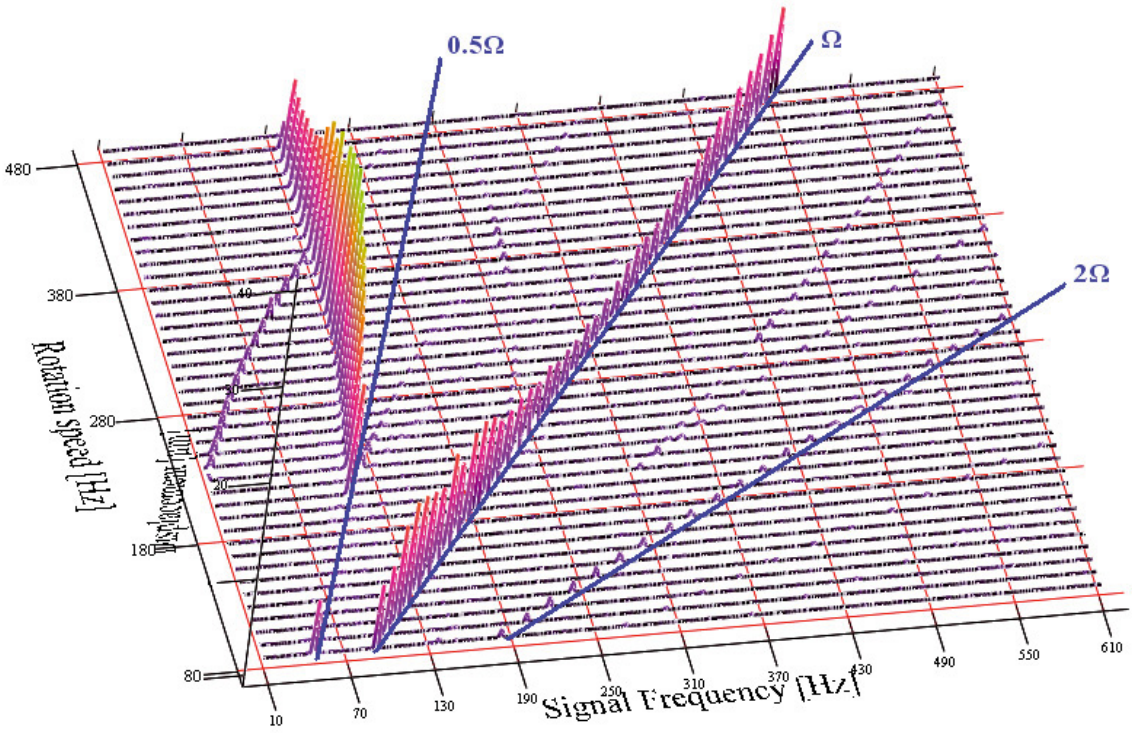

Fig. 7. Waterfall plot of a lightly loaded circular bearing (15 N).

Start-up check for the circular bearing was repeated with higher loads to find the static load corresponding to a stable bearing in the range of tested speeds. The static load should exceed 35 N in order to have a stable bearing up to 37 krpm.

Figure 8 shows a similar instability phenomenon detected during the start-up check of an unload foil bearing. In this case, self induced vibrations are represented as a whirl motion which appear at high rotational speed (>450 Hz). By applying 5 N of static load, the tested bearing recovers his stability up to 40 krpm which is the maximum allowable speed of its test rig.

5.2 Rotordynamic coefficients

5.2.1 Circular air bearing

The circular bearing was tested at two different speeds: 15 krpm and 35 krpm, and with two static loads: $W = 20$ N and $W = 40$ N respectively. Excitation frequencies were applied from 50 Hz to 400 Hz for the first working condition and up to 650 Hz for the second. For these tests, only the frequency of the excitations was imposed while it was verified that the amplitude of the dynamic force remained limited for avoiding any self induced vibrations.

Figure 9 shows the direct and cross-coupled dynamic coefficients for a 15 krpm running speed and 20 N of static force. Symbols represent the identified coefficient at each excitation frequency calculated by using Equation (3). In addition, this figure depicts the theoretical predictions [1]. Comparisons with theoretical data correlate well especially the cross-coupled coefficients. However measured direct coefficients (stiffness and damping) are slightly larger than theoretical predictions. The results show also a non linear dependence of the dynamic coefficients on the excitation frequency. Therefore, the smoothing procedure using the first order transfer function for a viscoelastic model (Eq. (6)) was used in order to plot continuous curves and to reduce measurement uncertainties. The smooth curve presented as a continuous line in Figure 9 was plotted using real or imaginary parts of the first order transfer functions of dynamic impedances Equation (7). Figure 10 shows a similar test with different working conditions ($\Omega = 35$ krpm and $W = 40$ N).

5.2.2 Air foil bearing

Figure 11 depicts the results of measurements performed at 15 krpm rotation speed and two static loads (20 N and 40 N). Excitation frequencies were applied from 80 Hz to 600 Hz. In the case of foil bearings, the excitation amplitude may also have an important influence on the dynamic coefficients due to the complying foil structure. Therefore the amplitude of the applied dynamic force was systematically kept constant at a value around 10 N for all tests.

Because the identified coefficients showed only a slight dependence on the excitation frequency, the values depicted in Figure 11 are directly stemming from Equation (4) without applying any smoothing procedure. In general, direct stiffness increases slightly or remains

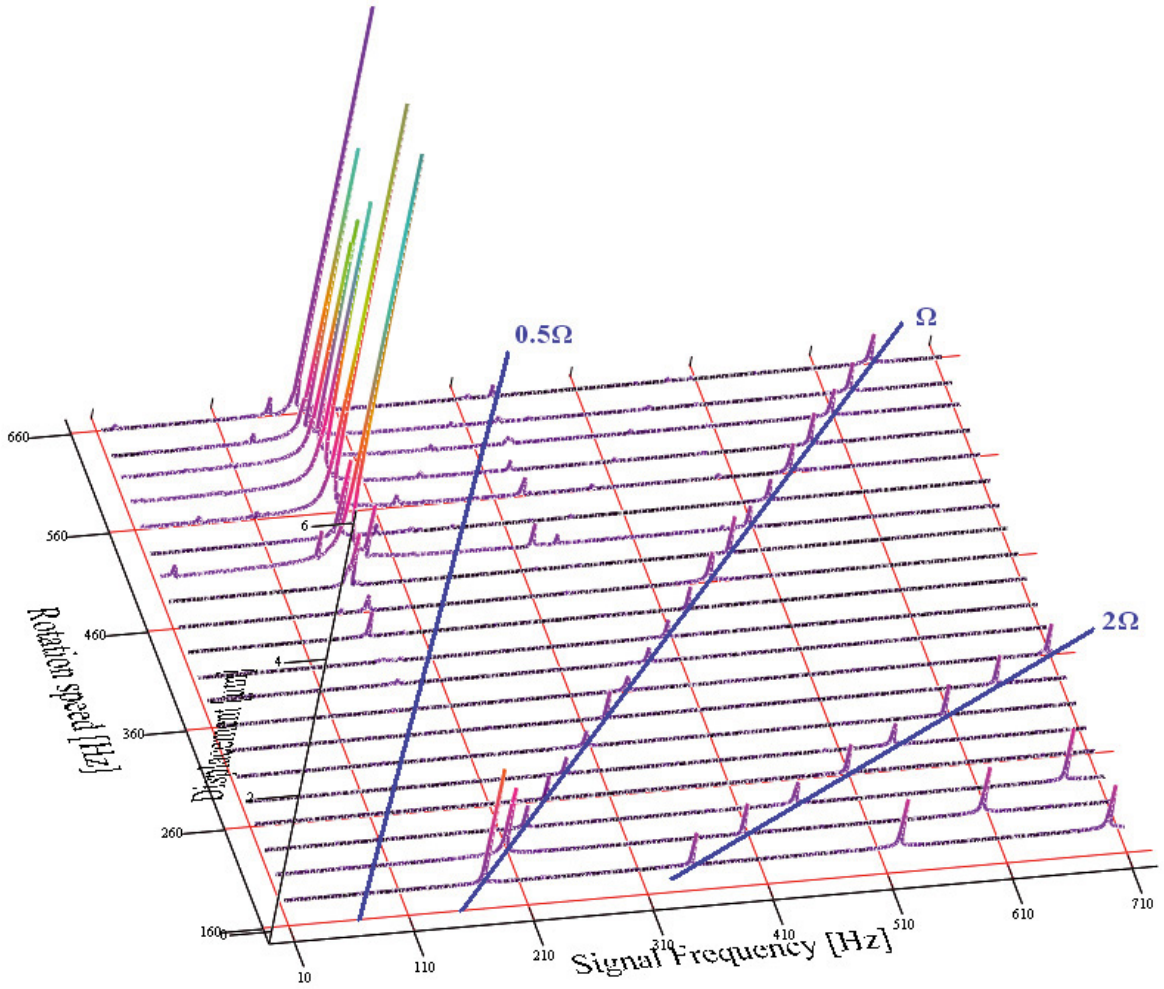

Fig. 8. Waterfall plot of an unloaded foil bearing.

constant while the cross coupling stiffness and all damping coefficients decrease with increasing the excitation frequency. Direct stiffness increases with increasing the static load. However, the static load has almost no influence on the damping coefficients. Figure 12 depicts the identified dynamic coefficients for the same static loads (20 N and 40 N) but for 35 krpm rotation speed.

An unexpected bend of the dynamic coefficient plots was observed in the vicinity of 400 Hz excitation frequency. This result was not a characteristic of the foil bearing but was identified as being a natural frequency of the support plates of the shakers. In fact as shown in Figure 1, each shaker is mounted on two plates that are flexibly mounted on the frame of the test rig with four low stiffness springs. By mounting additional accelerometers on the shaker supports a natural frequency of 380 Hz was subsequently identified.

This peculiar behaviour has also appeared for circular bearing investigations since the two test rigs use similar shakers supports. In this case, modal analysis has shown a natural frequency of 410 Hz. For this reason, Figures 9 and 10 show no rotor dynamic coefficients identification in the vicinity of 400 Hz.

6 Conclusion

The paper presents the experimental results obtained for a 40 mm circular bearing and a 38 mm first generation commercial foil bearing. Measurements were performed on two different test rigs using the same floating bearing design.

Results obtained for the circular bearing were compared to theoretical values and showed close correlation. In order to limit measurement uncertainties, a transfer function smoothing procedure was used. This method enables the representation of frequency-dependent bearing coefficients with continuous curves. The procedure developed for a simple, predictable bearing (circular bearing) was used in the analysis of the foil bearing that is expected to be a highly non linear component.

Comparison between the circular and the foil bearing enlightened the interest of the foil bearing technology. First, the lightly loaded (<5 N) foil bearing showed no self induced vibration in a large range of speeds (up to 40 krpm) which was a real advantage for the identification method. However, circular bearing generates instability at 20 krpm even with a relatively high static load

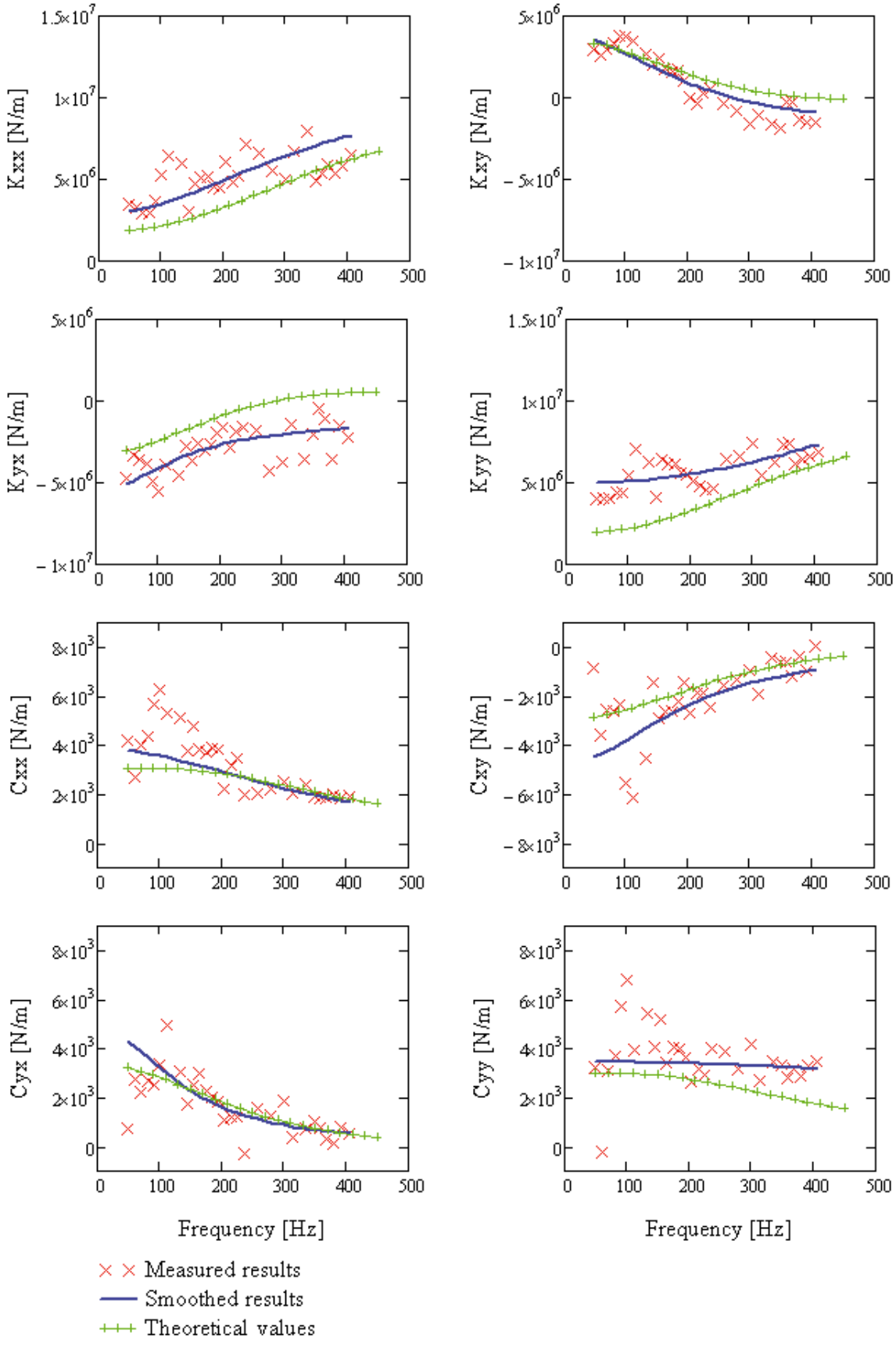

Fig. 9. Circular bearing dynamic coefficients ($\Omega = 15$ krpm, $W = 20$ N).

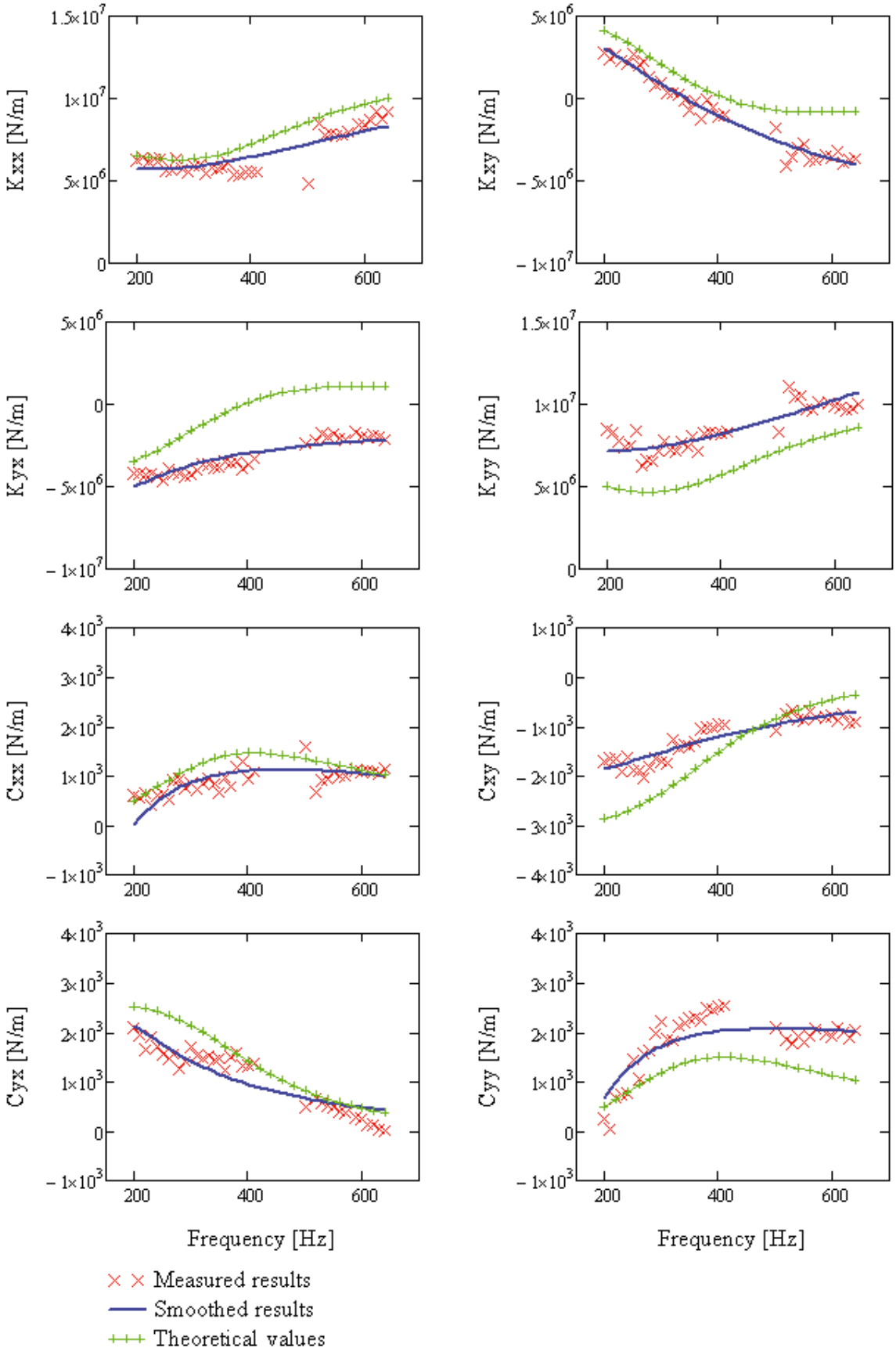

Fig. 10. Circular bearing dynamic coefficients ($\Omega = 35$ krpm, $W = 40$ N).

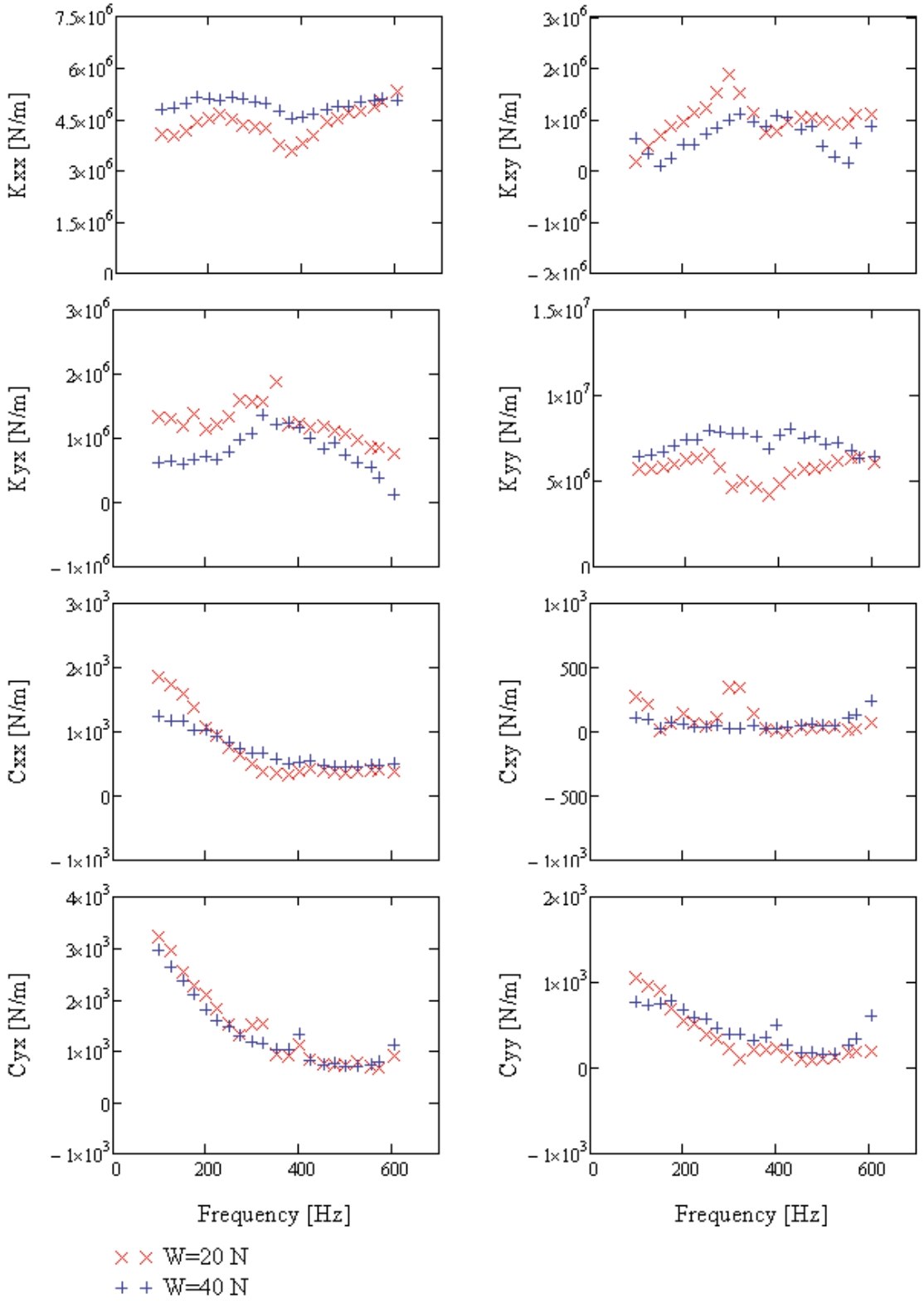

Fig. 11. Foil bearing dynamic coefficients ($\Omega = 15$ krpm).

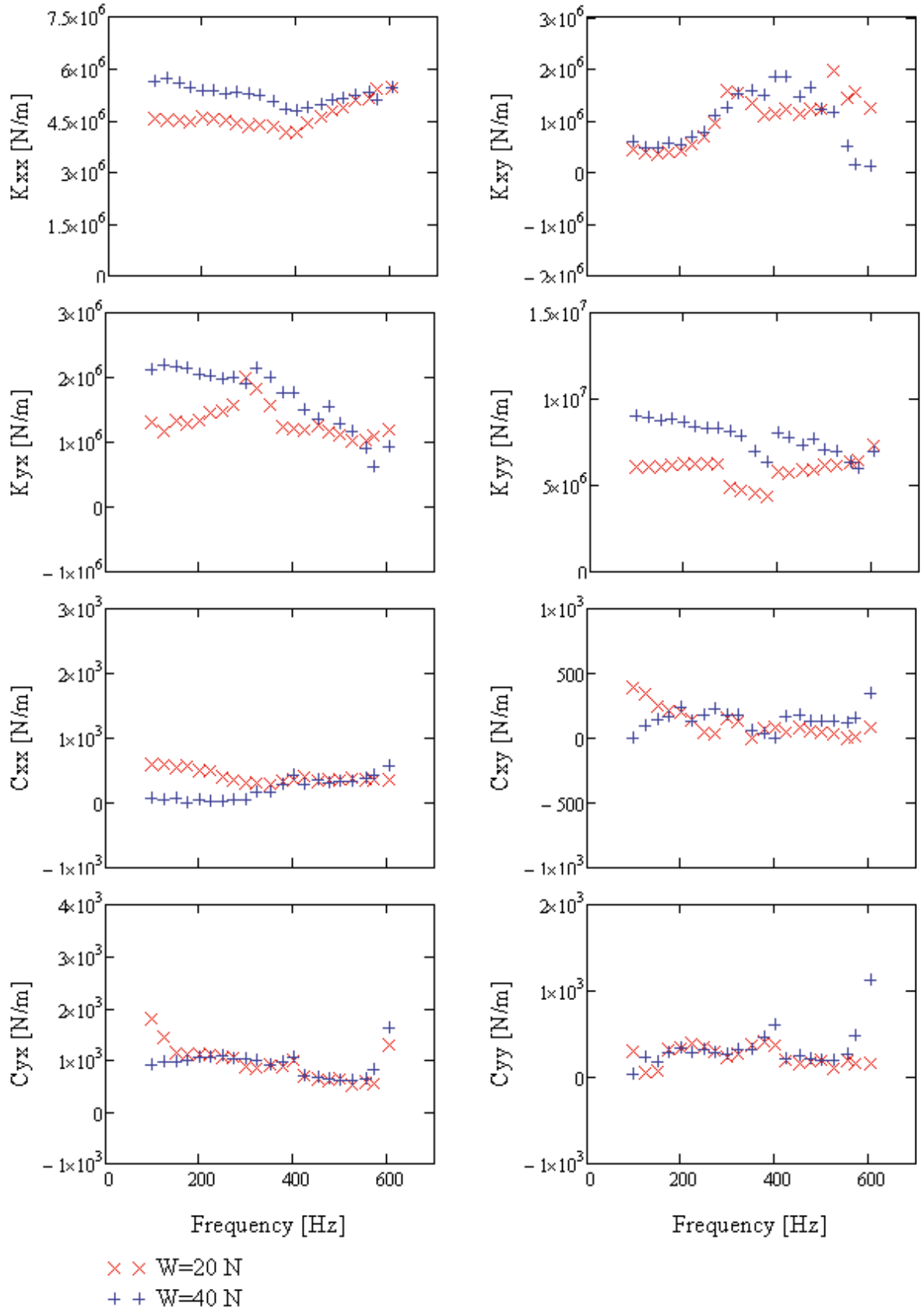

Fig. 12. Foil bearing dynamic coefficients ($\Omega = 35$ krpm).

(35 N). Identified rotordynamic coefficients show that both bearings have almost the same direct stiffness at low frequency excitation for the same working conditions. By increasing the excitation frequency, circular bearing direct stiffness increased which is not the case of foil bearing. Finally, the main advantage of foil bearing consists in conserving relatively high damping coefficients even at high frequency where circular bearing became almost an undamped component.

References

[1] S. Le Lez, Caractéristiques Statiques et Dynamiques des Paliers à Feuilles, Thèse de Doctorat, Université de Poitiers, 2007

[2] H. Heshmat, J. Walowit, O. Pinkus, Analysis of Gas-Lubricated Compliant Journal Bearings, ASME J. Lubr. Tech. 105 (1983) 647–655

[3] M. Carpino, G. Talmage, Prediction of Rotor Dynamic Coefficients in Gas Lubricated Foil Journal Bearings with Corrugated Sub-Foils, STLE Tribol. Trans. 49 (2006) 400–409

[4] L. San Andrés, T.H. Kim, Improvements to the Analysis of Gas Foil Bearings Integration of Top Foil 1d and 2d Structural Models, GT2007-27249, 2007

[5] S. Le Lez, M. Arghir, J. Frêne, Nonlinear Numerical Prediction of Gas Foil Bearings Stability and Unbalanced Response, ASME J. Eng. Gas Turbines Power 131 (2009) 012503–12

[6] G. Grau, Paliers aérodynamiques radiaux à structure à feuilles: Contribution à l'étude statique et comportement dynamique non linéaire, Thèse de doctorat, INSA de Lyon, 2004

[7] B. Ertas, M. Drexel, J. Van Dam, D. Hallman, A General Purpose Test Facility for Evaluating Gas Lubricated Journal Bearings, The 12th International Symposium on Transport Phenomena and Dynamics of Rotating Machinery, ISROMAC12-2008-20207, 2008

[8] B. Ertas, Compliant Hybrid Journal Bearings Using Integral Wire Mesh Dampers, GT2008-50984, 2008

[9] L. Rudloff, M. Arghir, O. Bonneau, P. Matta, Experimental Analysis of a First Generation Foil Bearing, Start-up Torque and Dynamic Coefficients, Proceedings of ASME Turbo Expo, GT2010-22966, 2010

[10] P. Matta, M. Arghir, O. Bonneau, Experimental Analysis of Cylindrical Air Bearing Dynamic Coefficients, Tribology Trans. 53 (2009) 329–339

[11] C. Rouvas, D.W. Childs, A Parameter Identification Method for the Rotordynamic Coefficients of a High Reynolds Number Hydrostatic Bearing, ASME J. Vib. Acoust. 115 (1993) 264–270

[12] L. San Andrés, S. Diaz, A Method for Identification of Bearing Force Coefficients and its Application to a Squeeze Film Damper With a Bubbly Lubricant, Tribology Trans. 42 (1999) 739–746

[13] M. Arghir, P. Matta, Compressibility effects on the dynamic characteristics of gas lubricated mechanical components, C. R. Mecanique (2009), doi:10.1016/j.crme.2009.09.002

[14] N. Geerts, Linear Dynamic Analysis of Rotorsystems with Gas Bearings, Master's thesis WFW-report 95.090, WFW, Faculty of Mechanical Engineering, Eindhoven University of Technology, 1995

[15] J.W. Roblee, Design of Externally Pressurized Gas Bearings for Dynamic Applications, Ph.D. Thesis, University of California, Berkley, CA, 1985

[16] L. San Andrés, Fluid Compressibility Effects on the Dynamic Response of Hydrostatic J. Bearings, Wear 146 (1991) 269–283

[17] G. Kleynhans, D. Childs, The Acoustic Influence of Cell Depth on the Rotordynamic Characteristics of Smooth-Rotor/Honeycomb-Stator Annular Gas Seals, ASME J. Eng. Gas Turbines Power 119 (1997) 949–957

[18] M. Fourka, Y. Tian, M. Bonis, Prediction of the stability of air thrust bearings by numerical, analytical and experimental methods, Wear 198 (1998) 1–6

[19] P. Matta, Analyse Expérimentale des Paliers Aérodynamiques, thèse de Doctorat, Université de Poitiers, 2009